Chemical Engineering Journal 155 (2009) 910–915

Contents lists available at ScienceDirect

Chemical Engineering Journal

journal homepage: www.elsevier.com/locate/cej

Zinc oxide nanostructures derived from a simple solution method for solar cells and LEDs

Periyayya Uthirakumar*, Hyung Gu Kim, Chang-Hee Hong*

School of Semiconductor Science and Chemical Technology, Semiconductor Physics Research Center, Chonbuk National University, Chonju 561-756, South Korea

ARTICLE INFO

Article history:
Received 13 July 2009
Received in revised form
15 September 2009
Accepted 19 September 2009

Keywords:
Oxides
Nanostructures
Chemical synthesis
Electron microscopy
Solar cells

ABSTRACT

A simple solution method has been proposed that deals the specific impacts of solvent characteristics on the growth of zinc oxide (ZnO) nanoparticles. The aggregation of particles is a major drawback in the hydrothermal method, and it is suppressed by using a less polar reaction solvent. ZnO particles obtained from a lower polarity indexed reaction medium show a very strong UV band-edge emission with an almost negligible deep level emission when compared to ZnO particles isolated from the higher polarity index of the medium. For the application is concerned, highly dispersible ZnO nanomaterials are used as an active material for dye-sensitized solar cells (DSSC), due to their higher internal surface area. Additionally, the deposition of ZnO layers on commercially available GaN-based blue light emitting diodes (LEDs) is fabricated to improve the light extraction efficiency, without disturbing the basic structure of the LED. The layer thickness and light transmission at a specific wavelength are the major factors which can improve the light emission from LEDs.

1. Introduction

Nanomaterials have attracted a great deal of attention due to their unique physical properties and promise for application in nanoscaled devices. Currently, there are extensive investigations into the control and manipulation of nanostructured materials. The field of nanostructures and their potential applications are rapidly expanding. Zinc oxide (ZnO) is a direct bandgap, wurtzite type semiconductor with an energy gap of 3.37 eV at room temperature. Due to its large bandgap, ZnO is an excellent semiconductor material for applications considered for other wide bandgap materials such as GaN and SiC. In addition, the excitons in ZnO are thermally stable at room temperature due to the extremely large exciton binding energy (about 60 meV), even higher than other semiconductor materials like GaN (25 meV) and ZnSe (22 meV). Thus ZnO has significant advantages in optoelectronic applications such as ultraviolet (UV) lasing, UV photonic devices, sensors and piezoelectric devices [1–3]. Also, the incorporation of few weight percentages of ZnO nanomaterials to the organic light emitting molecules could improve the emission properties significantly [4–8]. Because of their important potential applications, many recent investigations have focused on the synthesis and characterization of ZnO nanostructures including belts, wires, rods, tubes and cables [9–11]. In order to compete with conventional solid state processes, attention must be given to the preparation of micro- to nanoscaled ZnO particles through various synthetic routes, such as hydrothermal methods [12,13], thermal decomposition [14,15], and solution methods [16–19]. Such routes are attractive because of their mild synthetic conditions, low cost, and ease of mass production. Among them, a simple and effective method to obtain significantly crystallized nanomaterials could be a better alternative for future applications. In addition, selecting a cheap precursor with a relatively low operating temperature may further simplify nanomaterial synthesis.

Our group has recently reported a single-step process using simple solution techniques to synthesize a variety of ZnO nanoparticles from a single molecular precursor at very low temperature without assistance of base, surfactant, or a template [18,19]. Though we successfully synthesized micro- to nanosized ZnO materials, the major drawback of this system was the aggregation of fine ZnO nanoparticles, which eventually resulted in the formation of microsized particles. In general, materials in the form of aggregated particles do not always display the same characteristics as their nanoscale components; however, well-dispersed, individual crystallites can display their unique properties. Hence, we are intentionally working in this field to optimize a simple yet effective technique to synthesize very fine, individual ZnO nanoparticles. Consequently, we proposed a successful and simple system to prepare aggregation-free ZnO particles by selecting suitable reaction conditions, while keeping solvent properties in mind. This article mainly focuses on the synthesis and optical characterization of ZnO

* Corresponding authors. Tel.: +82 63 270 3928; fax: +82 63 270 3585.
E-mail addresses: uthirakumar@gmail.com (P. Uthirakumar), chhong@chonbuk.ac.kr (C.-H. Hong).

1385-8947/$ – see front matter © 2009 Elsevier B.V. All rights reserved.
doi:10.1016/j.cej.2009.09.025

Table 1
Summary of the reaction solvent characteristics and the morphologies of isolated ZnO particles.

Sample code	ZnHe	ZnXy	ZnEt	ZnMe
Primary solvent	Methanol	Methanol	Methanol	Methanol
Co-solvent	*n*-Hexane	*p*-Xylene	Diethyl ether	–
Total volume (ml)	25 + 25	25 + 25	25 + 25	50
Amount of zinc acetate (g)	0.05	0.05	0.05	0.5
Polarity index of solvents	5.1 + 0	5.1 + 2.5	5.1 + 2.8	5.1
Average polarity index	2.6	3.8	4.0	5.1
Water miscibility (%)	0.001	0.02	6.9	100
Extent of aggregation	No	No	No	Yes
Morphology	Snowflake-like	Sphere-like	Cage-like	Sphere-like

particles crystallized from non-polar hydrocarbon organic solvents and its applications toward DSSCs and LEDs.

2. Experimental

Zinc acetate dihydrate and solvents such as methanol, *n*-hexane, ether and *p*-xylene were purchased from Aldrich and used as received without further purification. In a typical procedure, 50 mg of zinc acetate dihydrate was dissolved completely in 25 ml of methanol, using ultra-sonication at room temperature. The clear transparent solution was diluted with an equal volume of (25 ml) of *p*-xylene and heated to 60 °C. The reaction was continued for about 10 h, while careful attention was paid not to lose any solvent by using a Liebig condenser. During this period of time, white ZnO particles were slowly crystallized and settled on the bottom of the flask. The white precipitate was filtered and washed with excess methanol at least three times to remove any starting materials or impurities and dried at 120 °C. Similarly, the other non-polar hydrocarbon solvents such as *n*-hexane and ether were used in place of *p*-xylene to investigate the specific impacts of solvent characteristics on the growth of the ZnO nanostructures. The detailed recipes are summarized in Table 1.

A dye-sensitized solar cell (DSSC) was fabricated as follows: highly dispersible ZnO nanoparticles were deposited over the pre-cleaned FTO substrate by a simple spin-coating technique. The as-prepared samples were annealed at 450 °C for 30 min, and then immersed in 0.3 mM N3 dye (*cis*-bis-(4,4′-dicarboxy-2,2′-bipyridine)dithiocyanato ruthenium(II), $Ru(dcbpy)_2(NCS)_2$) in ethanol for 24 h. A 50-μm-thick Surlyn frame was sandwiched between the open-pore side of the ZnO and a platinized FTO electrode. Light pressure was applied at 120 °C to seal the cell. A solution of 0.5 M LiI, 0.05 mM I_2, and 0.5 M *tert*-butylpyridine in 3-methoxypropionitrile was introduced into the cell via vacuum backfilling through a hole in the FTO electrode. Additional Surlyn and a microscope cover slip sealed the electrolyte into the cell. The active areas were limited to 0.04 cm^2 by the Surlyn frame and were masked from illumination by black electrical tape of the same dimensions. As far as light-emitting diodes (LEDs) are concerned, well-known blue light emitting InGaN–GaN epitaxial layers, mesa-structure LEDs with an area of 350 μm × 350 μm have been fabricated. A simple spin-coater was used to deposit very fine ZnO nanoparticles in a thin film on the blue LED chips to improve the light extraction efficiency of the device.

The surface morphologies of the as-prepared ZnO nanostructures were examined by field emission scanning electron microscopy (FESEM, Hitachi S-4700) and transmission electron microscopy (TEM, JEOL-2010). X-ray powder diffraction of the samples was obtained using a Rigaku X-ray diffractometer. X-ray diffractograms (XRD) were obtained using a Cu Kα incident beam (λ = 0.1546 nm), monochromated by a nickel filter. A Renishaw micro-Raman spectrometer RM 1000 with a visible 514 nm excitation laser was employed to measure the non-resonant Raman spectra of the ZnO samples. The number of gratings in the Raman spectrometer was 1800 for the visible laser. Photoluminescence (PL) measurements were carried out at room temperature at an excitation wavelength of 325 nm. The electrical characteristics of the prepared solar cell were investigated by measuring the current–voltage (*I*–*V*) behavior while the cells were irradiated by AM 1.5 simulated sunlight with a power density of 100 mW/cm^2. A high-speed LED tester and measurement system was used to measure the total luminous flux and radiometric power to compare the light extraction efficiency of the LEDs with or without ZnO nanoparticle layers through the help of a Keithley current source.

3. Results and discussion

The agglomeration effect is more prominent in aqueous media when compared to that in organic solvents [20]. Though organic solvents provide a better dispersing ability, they resulted in mostly aggregated nanoparticles. We have reported the simple solution methods for the preparation of ZnO nanoparticles from an organic polar solvent mixture. A full of ZnO nanoparticles were resulted as aggregates rather than as individual nanoparticles [19]. Hence, additional research is needed to isolate well-dispersed individual nanoparticles in organic solvent systems. Therefore, we intentionally investigated the causes of agglomeration in various organic solvents. Based on our earlier report, even after the formation of individual particles, aggregation begins with neighboring particles when the reaction medium has a water-miscible polar solvent, whose average polarity index is higher than 5.0 [19]. Similarly, if the reaction solution contains a water-immiscible non-polar solvent with an average polarity index lower than 5.0, then the extent of particle agglomeration is greatly controlled, leading to an individual nanoparticle in solution.

Here, one of three different water immiscible non-polar hydrocarbon solvents, *n*-hexane, *p*-xylene and ether, was mixed with a polar solvent (methanol), to reduce the average polarity of the medium. Three average polarities were generated, 2.6, 3.8 and 4.0, for each of the different solvent systems, designated ZnHe, ZnXy and ZnEt. The detailed solvent characteristics and experimental recipes are summarized in Table 1. When the average polarity of the reaction medium reached beyond a particular value, the individual nanoparticles started to aggregate themselves into relatively bigger particles. For example, ZnO isolated from ZnMe (average polarity index is 5.1) is full of aggregated ZnO nanoparticles ranging from 300 to 400 nm and it is difficult to find any individual particles [19]. But, at the same time, the ZnO obtained from a lower polarity indexed reaction medium showed well dispersed and stable ZnO nanoparticles. In particular with ZnXy, we were able to achieve well-dispersed, individual and stable ZnO nanoparticles by choosing the right combination of polar and non-polar solvents. The average particle size of the ZnO nanoparticles was 15 nm, and the reaction medium consisted of a mixture of methanol and xylene, with polarity indices of 5.1 and 2.5, respectively. Therefore, the average polarity index of the reaction medium was calculated to be 3.8, based on the formula (5.1 + 2.5)/2 in the ZnXy.

The morphological characteristics of the ZnO nanoparticles isolated from ZnXy were studied from scanning and transmission

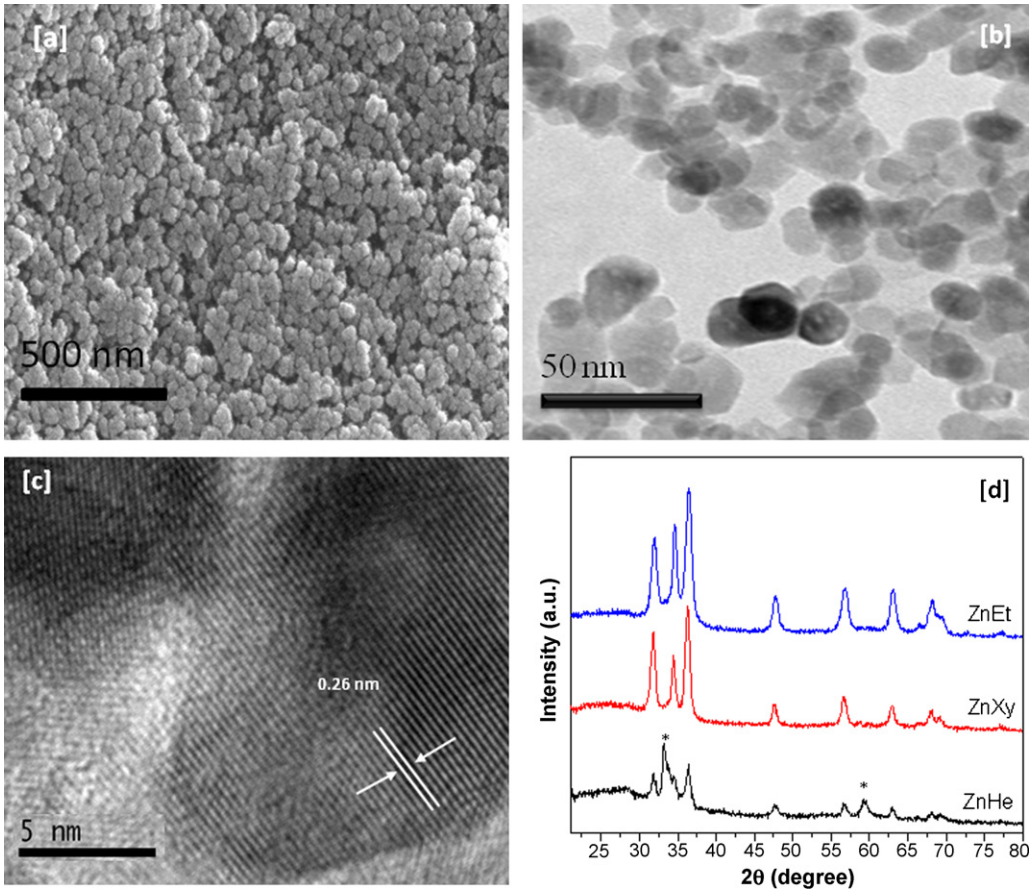

Fig. 1. Highly magnified (a) FESEM, (b) TEM and (c) HRTEM images of ZnO nanoparticles isolated from the mixture of methanol and xylene hydrocarbon solvent (ZnXy). (d) X-ray diffraction spectra of ZnO particles isolated from different types of solvent mixtures.

electron micrographs. Fig. 1 shows the highly magnified FESEM and TEM images of the ZnO nanoparticles of ZnXy. The FESEM pictures clearly show the uniform size distribution of the ZnO nanoparticles. Most of the crystals were found to be individual particles rather than agglomerated particles. The average particle size was approximately is noted to be 15 nm. This was further confirmed by the TEM images, as seen in Fig. 1(b and c). TEM images confirm the uniform nanoparticle distribution and the particle sizes are synchronized with the average particles sizes calculated from the FESEM pictures, with the help of scale bar provided. The lattice-resolved HRTEM images demonstrated that there were no crystalline defects such as dislocations and stacking faults present in the ZnO nanoparticles, as shown in Fig. 1(c). The spacing between the adjacent lattice planes was 0.26 nm, which corresponded with the distance between the two (0 0 0 2) crystal planes [21].

3.1. Effect of non-polar hydrocarbon solvents

Fig. 1(d) depicts the X-ray diffraction spectra of the ZnO particles crystallized with respect to different non-polar hydrocarbon solvent mixtures. The position of the XRD peaks along the different orientations showed the hexagonal wurtzite structure or phase of the ZnO, and the lattice constant values obtained from the XRD patterns of zinc oxide powders were in good agreement with the reported values [JCPDS Card No. 36-1451]. No typical diffraction peaks corresponding to other impurities were found in the ZnXy and ZnEt samples. However, a couple of new peaks appeared in the ZnHe, which corresponded to ZnO intermediates [$Zn_5(OH)_8(CH_3COO)_2$], as indicated by the star in Fig. 1(d) [17]. The appearance of ZnO intermediate peaks was probably a result of an incomplete decomposition of the zinc acetate precursor, due to the combined effects of a lower polarity index of the reaction medium and the immiscibility between the reaction solvents (methanol and *n*-hexane). In this case, solvent immiscibility between the two solvents significantly suppressed the rate of decomposition of the ZnO intermediates to form ZnO nanoparticles. Based on this information, at least a minimum polarity index and the solvent miscibility appeared to be essential to commence the decomposition of zinc acetate precursor to form a pure ZnO particle.

The high and low-magnified FESEM micrographs clearly show remarkably different morphologies of ZnO materials prepared from different non-polar hydrocarbon solvents, as shown in Fig. 2. The shape of the ZnO particles obtained from ZnHe resembled a snowflake-like structure. A special type of porous ZnO material morphology (cage-like) was observed from ZnEt. Very stable and aggregation-free ZnO nanoparticles were crystallized from ZnXy. On the contrary, fully agglomerated ZnO nanoparticles resulted from ZnMe, which was composed of very fine ZnO nanoparticles [19]. The individual particle sizes of the ZnHe, ZnXy, ZnEt and ZnMe were noted to be approximately 100 nm, 15 nm, 7 μm, and 17 nm, respectively. Fig. 3(a and b) represents the selected area electron diffraction (SAED) patterns of the ZnO nanoparticles synthesized from the ZnMe and ZnXy. The SAED patterns given in Fig. 3(a and b) reveal that the obtained ZnO particles were highly crystalline, in both cases. However, the density of bright spots present in Fig. 3(a) was much higher (ZnMe) than in Fig. 3(b) (ZnXy), which confirms the particle agglomeration in ZnMe. The corresponding TEM images of ZnMe and ZnXy were placed as an inset in Fig. 3(a and b). The particles seemed to be spherical in shape in both cases and the average particle sizes of ZnXy and ZnMe were observed to be around 15

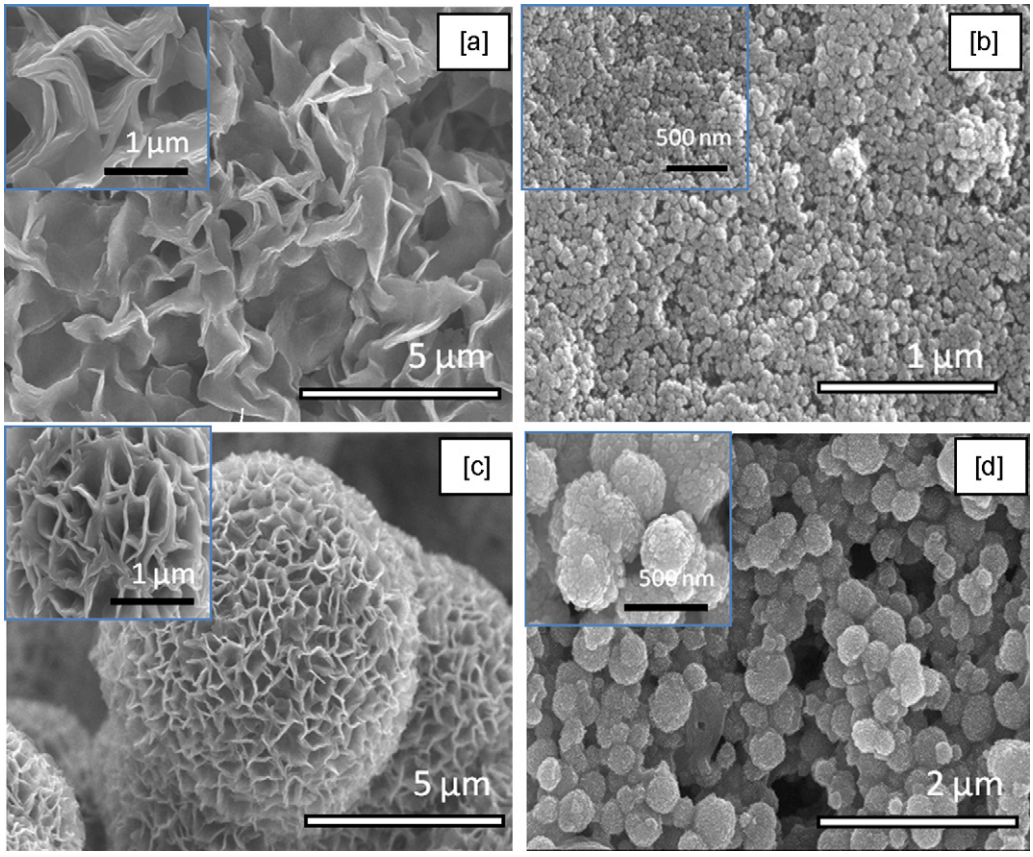

Fig. 2. Highly magnified FESEM images of ZnO particles isolated from (a) ZnHe, (b) ZnXy, (c) ZnEt and (d) ZnMe. The insets are the respective low-magnified FESEM images.

and 17 nm, respectively. Although there was not much difference in their particles sizes, agglomeration led to the larger sizes of over 300–400 nm in the ZnMe, as shown in the TEM image. Based on these observations, a new question arises regarding the cause of the particle agglomeration between the ZnMe and ZnXy. Possible causes are (i) the average polarity index and (ii) the water miscibility of reaction medium. The average polarity index and water miscibility values of ZnMe and ZnXy were 5.1, 100 and 2.8, 0.02, respectively.

The extent of the ZnO nanoparticle aggregation between the ZnMe and ZnXy was studied by the following simple technique. A known amount of ZnO nanoparticles was dispersed in a desired volume of methanol. The dispersed mass was ultra-sonicated for 15 min and allowed to sit for about 48 h to observe the dispersion ability in methanol. A photograph was taken after 48 h, as shown in Fig. 3(c). Here, ultra-fine ZnO nanoparticles from ZnXy show a very stable dispersion in methanol, even after 48 h. However, the ZnO nanoparticles from ZnMe had completely settled on the bottom of the glass vial, as shown in Fig. 3(c). A stable dispersion of ZnXy is much more useful in making a very thin and effective ZnO layers for various applications such as in LEDs or solar cells.

The room temperature photoluminescence spectra (PL) of ZnO particles were prepared in different solvents at an excitation wavelength at 325 nm and are shown in Fig. 3(d). It is well known that the room temperature PL spectra of ZnO show three major peaks, a UV near band-edge emission around 380 nm, a green emission peak around 520 nm and a red or orange emission around 600 nm [21]. The appearances of band-edge and deep level (DL) emissions are due to the occurrence of free-exciton recombination and structural defects, respectively [22,23]. ZnXy showed a very strong UV band-edge emission with almost no DL emission peak which indicated high-purity ZnO nanoparticle formations. However, there was a broad PL signal observed in the range from 500 to 700 nm, along with a UV band-edge emission in both the ZnHe and ZnEt. The wide PL signal was attributed to excitonic PL, which mainly resulted from the surface oxygen vacancies and structural defects. The presence of a sharp PL signal at 380 nm was responsible for the perfect growth of the ZnO particles. In comparison with the PL spectrum of ZnMe, a broader PL signal was observed in the visible region with almost no characteristic UV band-edge emission at 380 nm [19]. These results confirmed that the structurally defective ZnO particles were mainly obtained from a highly polar solvent medium, while a perfect ZnO crystal occurred in the lower polarity solvent mixture.

The Raman spectra of the ZnO samples are shown in Fig. 4. The most common Raman active peaks were observed at 330, 439, and 583 cm^{-1} in all of the samples and were assigned to the various Raman active modes of the ZnO particles. The peak at 439 cm^{-1} was attributed to the ZnO non-polar optical phonon E_2 mode and the peak at 583 cm^{-1} was assigned to the E_1 (LO) mode of the ZnO. It is widely believed that the appearance of the E_{1L} mode in Raman scattering is due to the impurities and structural defects (oxygen vacancies and Zn interstitials) of the deposited products. Apart from these peaks, a sharp and strong peak at around 330 cm^{-1} (A_1) was indicative of the material responsible for the formation of single crystalline ZnO particles [24].

Overall, two important key factors have been revealed, the average polarity index of the reaction medium and the water miscibility. In the former case, when the average polarity index of the reaction mixture falls below three, the rate of decomposition of the zinc acetate precursors is comparably slow, leading to incomplete precursor decomposition and a thus reduced generation of pure ZnO particles (ZnHe). At the same time, when the average polarity index exceeds five, though the formation of very fine ZnO nanoparticles still occurred, aggregation took place and

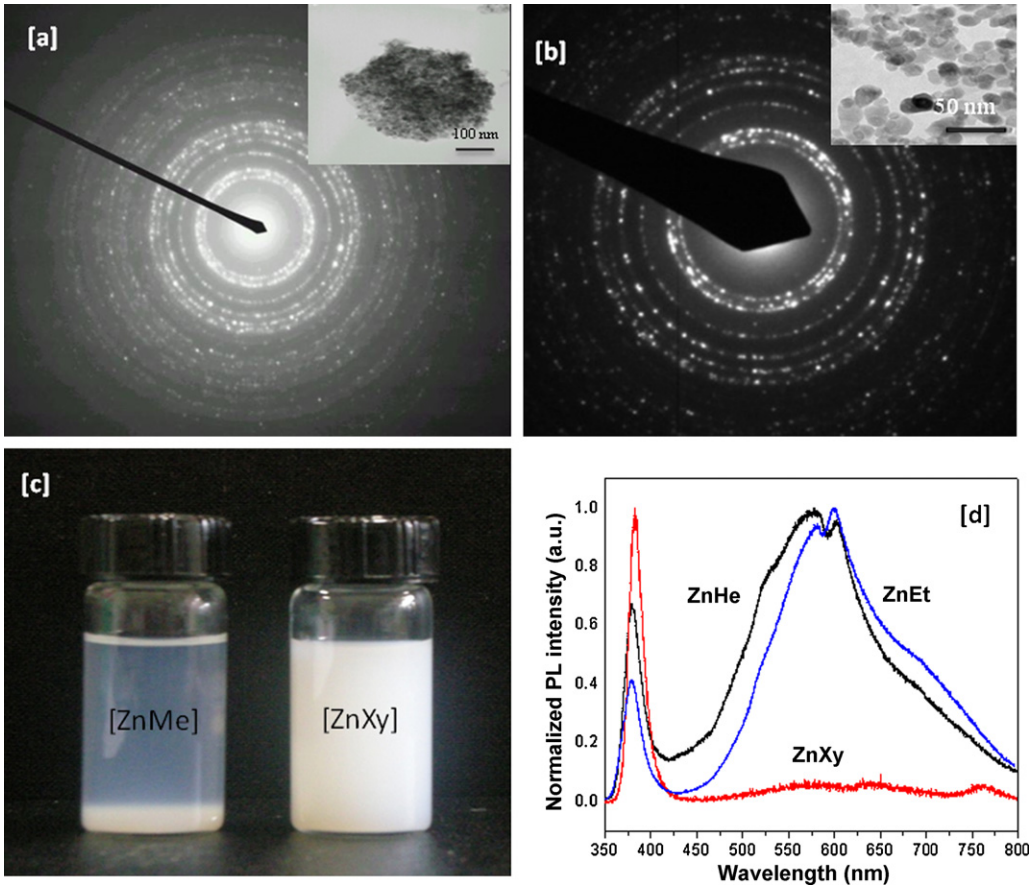

Fig. 3. SAED pattern of ZnO nanoparticles from (a) ZnMe and (b) ZnXy [the corresponding TEM images are displayed as insets]. (c) A photograph showing the dispersion ability of the ZnO nanoparticles isolated from ZnMe and ZnXy [photo was taken after 48 h in methanol]. (d) Room temperature photoluminescence spectra of ZnO particles isolated from ZnHe, ZnXy and ZnEt.

larger particles began to develop (ZnMe). Therefore, based on these experimental results, the optimum level for the average polarity index should fall between 3.5 and 4.0. Similarly, water miscibility plays an important role in particle aggregation. Water-immiscible xylene solvents provided better dispersion than the water-miscible methanol, which induced agglomeration. Thus, in order to produce individual nanoparticles, careful attention has to be paid to the selection of the right combination of organic solvent mixture. This simple method could be the best approach to achieve highly dispersible, free-standing, stable ZnO nanoparticles in a solution technique, preferable over to the hydrothermal methods.

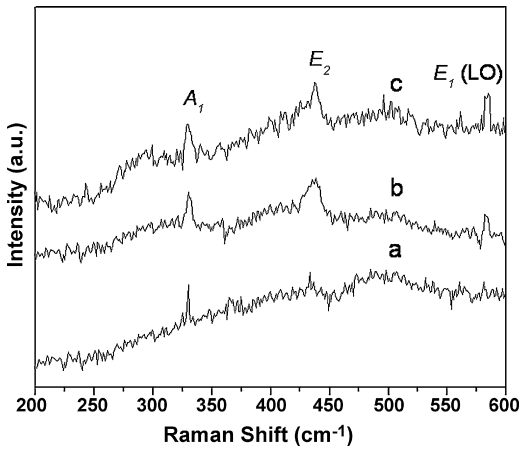

Fig. 4. Raman spectra of ZnO particles isolated from (a) ZnHe, (b) ZnXy and (c) ZnEt.

3.2. For dye-sensitized solar cells

A DSSC device was fabricated using ZnO nanoparticles obtained using ZnXy as an active layer. The current density–voltage (J–V) behavior was measured while the cells were irradiated by AM 1.5 simulated sunlight with a power density of 100 mW/cm^2, to investigate the performances of the DSSC device. Fig. 5(a) shows the photocurrent density *vs.* voltage curves. The power conversion efficiency (PCE) was calculated from the equation, PCE (η) = $J_m V_m / P_{inc}$, where J_m is the maximum current, V_m is the maximum voltage, and P_{inc} is the incident light power. The DSSC fabricated with ZnXy nanoparticles showed the short circuit current (J_{sc}) of 5.4 mA/cm^2, the open circuit voltage (V_{oc}) of 0.51 V, the fill factor (FF) of 0.43%and PCE value of 1.166%. The relatively higher PEC value is observed in ZnXy nanoparticles when compared to ZnO nanopowder (0.68%), nanobelt (0.29%) and nano-tetrapod (0.41%) [25]. Higher surface area of the ZnO nanoparticles promoted to improve large number of adsorption of the dye molecules led higher light harvesting [26]. Also, the multiple light scattering is responsible for the relatively higher PCE, due to the photoinduced lasing emission on closely packed ZnO particles [27]. In addition, ZnO nanoparticles dispersion was used as a buffer layer for polymer solar cell (PSC), due to better compatibility between the hydrophobic polymer layer and hydrophilic ink [28].

3.3. For light emitting diodes

For LED applications, the light extraction efficiency of the device was improved by deposition of ZnO nanoparticle (ZnXy) layers

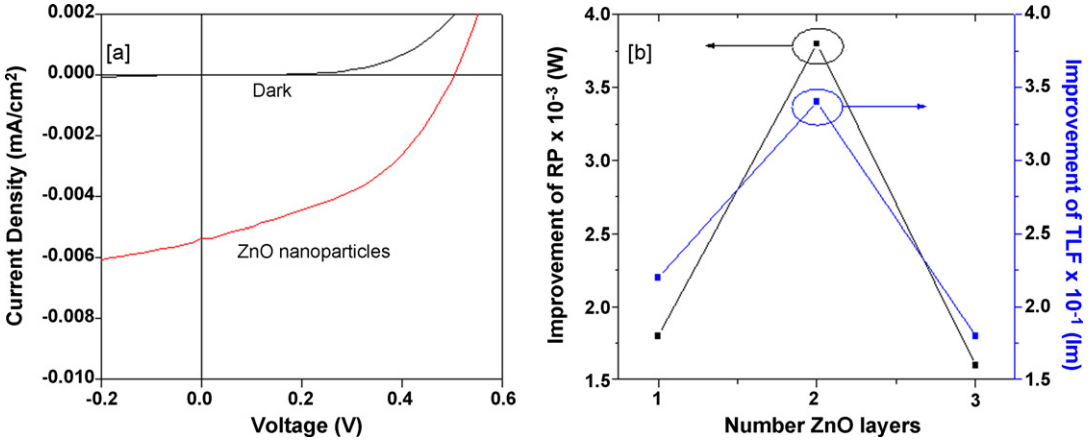

Fig. 5. (a) Current density against voltage (*J–V*) characteristics of ZnXy nanoparticles used in dye-sensitized solar cells and (b) the improvement of light output power with respect to the number of ZnXy nanoparticle layers on blue LED.

onto the commercially available GaN-based blue LED. Well-known blue light emitting InGaN–GaN epitaxial layers, mesa-structure LEDs with an area of 350 μm × 350 μm have been fabricated, and a simple spin-coater was used to deposit the ZnO nanoparticles dispersed in methanol. To improve the light extraction efficiency (LEE) of the device, one, two and three layers of ZnO nanoparticles were coated onto the blue LED. The layer thickness and the light transmittance at a specific wavelength are the key factors to consider. The film thickness was increased from the one to three layers, obviously, while the percentage of light transmittance was decreased. The light output power of the LEDs before and after ZnO-layer addition was measured by a high-speed LED tester and measurement system. Fig. 5(b) shows the improvement in radiometric power (RP) and total luminous flux (TLF) of the device with respect to number of ZnO layers. Interestingly, the RP and TLF were observed to have maximum improvements of 3.8 and 3.4%, respectively, with the double ZnO layer sample, when compared to a bare blue LED chip. A higher LEE of the ZnO nanoparticles was attributed to increased surface roughness that likely caused angular randomization of the photons, leading to a higher probability of photon escape from the LED. Thus, this increased the integrated intensity along with the graded refractive index matching from the blue LED to air through the ZnO nanoparticles.

4. Conclusions

Highly dispersible ZnO nanoparticles have been successfully synthesized by controlling the reaction solvent characteristics at a relatively low temperature in a simple solution method. Two important solvent characteristics of polarity index and water miscibility of the hydrocarbon solvent were discussed. The average polarity index of the reaction medium controlled the decomposition of the zinc acetate precursors and thus their ability to generate pure ZnO particles. Water miscibility was shown to be important in particle aggregation. Very slow crystallization of ZnO particles in the non-polar hydrocarbon solvents was responsible for the UV band-edge emission. A stable ZnO nanoparticle dispersion was used as an active component in DSSC, along with an excellent graded index material, to improve the light extraction efficiency in GaN-based LEDs.

Acknowledgement

This work was supported by the Korea Research Foundation Grant funded by the Korea Government (KRF-2008-005-J00301)

References

[1] M.H. Huang, S. Mao, H. Feick, H.Q. Yan, Y.Y. Yu, H. Kind, R. Russo, P.D. Yang, Science 292 (2001) 1897.
[2] X. Liu, X. Wu, H. Cao, R.P.H. Chang, J. Appl. Phys. 95 (2004) 3141.
[3] H. Cao, Y.G. Zhao, S.T. Ho, E.W. Seelig, Q.H. Wang, R.P.H. Chang, Phys. Rev. Lett. 82 (1999) 2278.
[4] P. Uthirakumar, C.H. Hong, E.K. Suh, Y.S. Lee, Chem. Mater. 18 (2006) 4990.
[5] P. Uthirakumar, E.K. Suh, C.H. Hong, Y.S. Lee, J. Appl. Polym. Sci. 102 (2006) 5344.
[6] P. Uthirakumar, Y.S. Lee, E.K. Suh, C.H. Hong, J. Lumin. 128 (2008) 287.
[7] P. Uthirakumar, E.K. Suh, C.H. Hong, Thin Solid Films 516 (2008) 7299.
[8] P. Uthirakumar, E.K. Suh, C.H. Hong, J. Lumin. 128 (2008) 1629.
[9] Y. Zhang, N. Wang, S. Gao, Chem. Mater. 14 (2002) 3564.
[10] Z.W. Pan, Z.R. Dai, Z.L. Wang, Science 291 (2001) 1947.
[11] J.Q. Hu, Q. Li, X.M. Meng, C.S. Lee, S.T. Lee, Chem. Mater. 15 (2003) 305.
[12] D.R. Chen, X.L. Jiao, G. Cheng, Solid State Commun. 113 (2000) 363.
[13] T. Sekiguchi, S. Miyashita, K. Obara, T. Shishido, N. Sakagami, J. Cryst. Growth 214/215 (2000) 72.
[14] M.S. Niasari, N. Mir, F. Davar, J. Alloy Compd. 476 (2009) 908.
[15] M.S. Niasari, F. Davar, Z. Fereshteh, Chem. Eng. J. 146 (2009) 498.
[16] J. Zhang, L. Sun, J. Yin, H. Su, C. Liao, C. Yan, Chem. Mater. 14 (2002) 4172.
[17] H. Wang, C. Xie, D. Zeng, J. Cryst. Growth 277 (2005) 372.
[18] P. Uthirakumar, Y.-S. Lee, E.-K. Suh, C.-H. Hong, Phys. Lett. A 359 (2006) 223.
[19] P. Uthirakumar, B. Karunagaran, S. Nagarajan, E.-K. Suh, C.-H. Hong, J. Cryst. Growth 304 (2007) 150.
[20] C.L. Pueyo, M.W.E. van den Berg, A.D. Toni, T. Goes, S. Polarz, J. Am. Chem. Soc. 130 (2008) 16601.
[21] S.A. Studenikin, N. Golego, M. Cocivera, J. Appl. Phys. 84 (1998) 2287.
[22] W.F. Zhang, M.S. Zhang, Z. Yin, Q. Chen, Appl. Phys. B 70 (2000) 261.
[23] K. Vanheusden, W.L. Waren, C.H. Seager, D.R. Tallant, J.A. Voigt, J. Appl. Phys. 79 (1996) 7983.
[24] Y.H. Yang, C.X. Wang, B. Wang, N.S. Xu, G.W. Yang, Chem. Phys. Lett. 403 (2005) 248.
[25] S. Choopun, A. Tubtimtae, T. Santhaveesuk, S. Nilphai, E. Wongrat, N. Hongsith, Appl. Surf. Sci., Available online 9 June 2009, doi:10.1016/j.apsusc.2009.05.139.
[26] J.B. Baxter, E.S. Aydil, Appl. Phys. Lett. 86 (2005) 053114.
[27] H. Cao, J.Y. Xu, D.Z. Zhang, S.H. Chang, S.T. Ho, E.W. Seelig, X. Liu, R.P.H. Chang, Phys. Rev. Lett. 84 (2000) 5584.
[28] S.H. Eom, S. Senthilarasu, P. Uthirakumar, C.-H. Hong, Y.-S. Lee, J. Lim, S.C. Yoon, C. Lee, S.-H. Lee, Sol. Energy Mater. Sol. Cells 92 (2008) 564.